the plant journal

SEB SOCIETY FOR EXPERIMENTAL BIOLOGY

The Plant Journal (2026) **128,** e71256 doi: 10.1111/tpj.71256

Genetic dissection of kernel dehydration traits in maize using a recombinant inbred line population: key loci and candidate genes

Dan Yang[1,2], Hetian Wang[1,2], Yong Peng[1], Yun Luo[1], Yuancheng Xu[1], Lijun Zhao[1], Luxi Wang[1], Junpeng Zhan[1,2], Yingjie Xiao[1,2], Jianbing Yan[1,2] and Wenqiang Li[1,2,*]

[1]*National Key Laboratory of Crop Genetic Improvement, Hainan Research Institute, Huazhong Agricultural University, Wuhan 430070, Hubei, China, and*

[2]*Hubei Hongshan Laboratory, Wuhan, Hubei 430070, China*

Received 23 April 2026; revised 28 October 2026; accepted 4 November 2026.

*For correspondence (e-mail liwenqiang0111@mail.hzau.edu.cn).

SUMMARY

High kernel moisture content (KMC) at harvest impedes mechanized harvesting of maize and increases production costs. As a complex trait influenced by both genetic and environmental factors, kernel moisture dynamics can be quantified using three key metrics: KMC, kernel dehydration rate (KDR), and area under the dry-down curve (AUDDC). Here, we evaluated the dynamic changes of kernel moisture across five consecutive stages in a KD recombinant inbred line population across five environments. KMC was measured every 5 days from 34 to 58 days after pollination (DAP), and KDR and AUDDC were calculated based on these measurements. Quantitative trait locus (QTL) mapping identified 100 non-redundant QTLs, mainly located at distal chromosomal regions. Of these, we prioritized environmentally stable QTLs and 9 high-confidence pleiotropic candidate regions controlling all 3 kernel dehydration traits, alongside trait-specific loci unique to KMC (11), KDR (28), and AUDDC (4). Meanwhile, combined with RNA-seq data and published literature, we further identified 982 genes differentially expressed between the parental lines at the late stage of kernel development within these 100 QTL intervals. The colocalization of our QTLs with meta-QTLs (11 for GDR and 34 for GWC) revealed 13 high-confidence conserved genomic regions, among which 2 prioritized candidate genes (*Zm00001d002455* and *Zm00001d005798*) were identified. Our study integrated QTL mapping, genome-wide association studies, and transcriptomic analysis to identify high-confidence pleiotropic QTLs and key candidate genes regulating maize kernel moisture, revealing the genetic architecture of moisture dynamics and supporting the breeding of fast-dehydrating maize varieties.

Keywords: maize, QTL, kernel dehydration, candidate gene, regulatory pathway.

INTRODUCTION

Maize (*Zea mays* L.), being one of the most important crops worldwide, acts as a fundamental source for feed, food, energy, and industrial raw materials (Emes et al., 2003; Qu et al., 2022; Xie et al., 2022). Mechanized harvesting has become an inevitable trend in major maize-producing countries worldwide (Acemoglu & Restrepo, 2022; Mizik et al., 2025; Trinh Thi & Zhou, 2024; Wang, Shen, & Cai, 2025; Yang et al., 2025). However, a common challenge limiting the efficiency of mechanical grain harvesting is high kernel moisture content (KMC) at harvest, which leads to elevated kernel breakage rates, potential mechanical blockage, prolonged post-harvest drying duration, increased grain production costs, and reduced farming incomes (Li et al., 2025; Wang, Li, et al., 2021; Xin et al., 2024; Yang et al., 2023). This issue is particularly pronounced in China. According to the US Grains Council reports covering 2020–2025 harvest seasons, average harvest kernel moisture in the United States has remained stable at 16.0%, fluctuating from 15.3 to 16.3% (US Grains Council, 2026); whereas in China, large-scale survey data collected from 2012 to 2019 reported an average harvest KMC of 25.9% (Wang, Li, et al., 2021). Such moisture levels exceed the recommended threshold for efficient mechanical harvesting and cost-effective, safe grain storage (Fang et al., 2019; Keru et al., 2022; Yang et al., 2023).

Kernel dehydration rate (KDR) is a key factor influencing KMC at harvest, as it directly reflects the speed of moisture loss during kernel development and is regulated

© 2026 The Author(s).
The Plant Journal published by Society for Experimental Biology and John Wiley & Sons Ltd.
This is an open access article under the terms of the Creative Commons Attribution License, which permits use, distribution and reproduction in any medium, provided the original work is properly cited.

by both genotype and environment (Dodig et al., 2008; Jia et al., 2020; Purdy & Crane, 1967; Wang et al., 2022). The area under the dry-down curve (AUDDC), a derivative trait quantifying cumulative moisture dynamics, also correlates with KMC; a larger AUDDC value indicates slower dehydration and higher final moisture content (Li et al., 2021; Yang et al., 2010). Specifically, KDR is influenced by factors such as the water content of maize husks, the moisture content of the cob, the tightness of the husks, the number of husks, and the length of the husks (Dai et al., 2019; Li et al., 2016; Liu et al., 2023; Zhou et al., 2020). In addition, KDR is also affected by a series of environmental factors, including air humidity, temperature, daily radiation, wind speed, rainfall, and planting density (Cross, 1991; Widdicombe & Thelen, 2002). AUDDC reflects the trend of water content during kernel development. In conclusion, increased KDR and reduced AUDDC/KMC are important for achieving KMCs desired for mechanical harvesting of maize.

The development of maize kernels starts with double fertilization (Dai et al., 2021), and kernel filling is a crucial and continuous stage that has a profound impact on the yield and quality at harvest (Gao et al., 2025). In fact, kernel dehydration starts from the kernel-filling stage and lasts throughout the entire kernel-filling process (Brooking, 1990). Firstly, during the lag phase, the kernels absorb water rapidly and expand in volume (Borrás & Westgate, 2006; Brooking, 1990). After entering the linear kernel-filling phase, the kernels continue to absorb water at first, and then begin to experience net water loss after reaching the peak, which is an important stage for the rapid accumulation of dry matter (Alam et al., 2021; Borrás & Westgate, 2006). Finally, at physiological maturity, the kernel weight reaches its peak, and water loss shifts from a physiological to a physical process (Gao et al., 2021). Therefore, KMC, KDR, and AUDDC are all very complex traits that are greatly influenced by quantitative trait locus (QTL) and environmental conditions (Liu et al., 2020).

There have been many studies on KMC, KDR, and AUDDC, among which most are focused on related QTL identification (Capelle et al., 2010; Li et al., 2021; Qian et al., 2016; Sala et al., 2012; Yin et al., 2020; Zhang, Zhang, et al., 2020). Valérie Capelle et al. used an intermated RIL population to identify 78 QTLs related to kernel desiccation, kernel weight, and abscisic acid (ABA) content in 2010, and multi-QTL models explained 35–50% of the phenotypic variation for traits related to water status (Capelle et al., 2010). Sala et al. identified 34 MetaQTL associated with KMC when evaluating inbred lines *per se* (LP) and test crosses (TC) data (Sala et al., 2012). Yin et al. identified 76 QTLs related to dehydration through a recombinant inbred line (RIL) population, accounting for 1.03–15.24% of the phenotypic variation (Yin et al., 2020). Qian et al. used a permanent F_2 generation population to identify five QTLs, of which the phenotypic variation contribution is ≥10% (Qian et al., 2016). Li et al. used 513 diverse maize inbred lines to reveal 71 QTLs related to KMC and pinpointed two candidate genes, *GRMZM5G805627* and *GRMZM2G137211* (Li et al., 2021). Zhang et al. used the AUDDC method to evaluate a single-cross population, identifying four QTLs that can explain more than 10% of phenotypic variance (Zhang, Zhang, et al., 2020). Notably, a recent study identified subclass III ZmSnRK2s (e.g., *ZmSnRK2.10*) as key regulators of kernel dehydration, demonstrating that *ZmSnRK2.10* overexpression accelerates dehydration and reduces KMC at physiological maturity through an ABA–SnRK2–bZIP signaling pathway (Wang, Long, et al., 2025). However, relatively few studies have confirmed major QTLs and candidate genes, making it difficult to utilize the QTLs in breeding (Wang, Long, et al., 2025; Yu et al., 2025). This study employs the identical K22 × DAN340 KD RIL population utilized by Yu et al. (2025), who functionally validated the single locus *qKDR1*. Unlike their single-gene-focused research, we conduct multi-environment, dynamic genome-wide QTL mapping for three interconnected kernel dehydration traits, establishing a comprehensive global genetic framework for this population and verifying the reliability of our QTL detection pipeline via overlap with *qKDR1* (Yu et al., 2025).

RESULTS

Abundant diversity in kernel moisture content traits within the KD RIL population

The two parental lines of the KD RIL population (K22 and DAN340) showed significant differences in KMC (Figure 1a). Analysis of moisture changes across different locations (Figure S1) revealed that DAN340 had a significantly higher initial KMC than K22 in some environments but a lower final KMC and faster dehydration rate—a pattern contributing to rich phenotypic diversity in their progeny across varying environments. For the KD RIL population, phenotypic analysis showed that KMC, KDR, and AUDDC all followed a normal distribution (Figure S2). Furthermore, KMC showed significant variation across time points and geographical environments. Overall, the average KMC showed a continuous downward trend from the early to late stages, but the decreasing trends differed in various environments (Figure 1b). Furthermore, the best linear unbiased prediction (BLUP) values showed that average KMC decreased consistently over time, from 46.05% at 34 DAP to 26.42% at 58 DAP (Tables S1 and S6). Across all environments, average KMC followed a similar decreasing trend, with initial values ranging from 40.18 to 54.03% at 34 DAP and final values from 18.86 to 34.51% at 58 DAP. Notably, in the 13HN environment, the average KMC kept decreasing, from 54.03% at 34 DAP to 25.13% at 58 DAP. In the 14JL environment, the average KMC kept decreasing, from 47.06% at 34 DAP to 34.51% at 58 DAP. This extensive

© 2026 The Author(s).

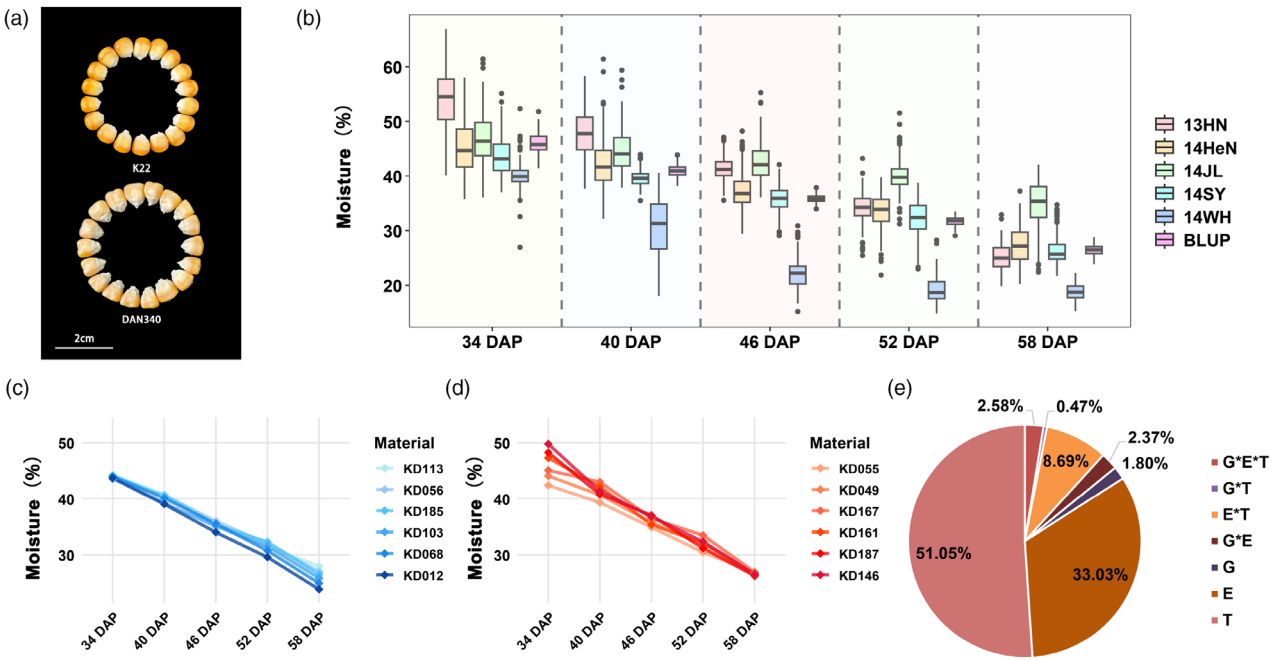

Figure 1. The phenotypic dynamics and variance components of kernel dehydration traits.
(a) Representative kernels of parental lines K22 and DAN340 at 45 days after pollination (DAP), arranged concentrically (Bar = 2 cm).
(b) Phenotypic distribution of kernel moisture content (KMC) across five geographic environments and best linear unbiased prediction (BLUP) estimates, stratified by developmental stage (34–58 DAP). Boxplots are ordered by ascending latitude, revealing progressive moisture decline in all environments.
(c) Representative dehydration trajectories of recombinant inbred lines (RILs) (blue lines) selected to illustrate lines with similar initial KMC at 34 DAP but divergent final KMC at 58 DAP.
(d) Representative dehydration trajectories of RILs (red lines) selected to illustrate lines with divergent initial KMC but convergent final KMC.
(e) Variance partitioning via three-way ANOVA, attributing KMC variation primarily to time (T, 51.05%) and environment (E, 33.03%), with minor contributions from genotype (G, 1.8%) and interactions (G × E, G × T, E × T, G × E × T).

phenotypic variation underscores the complex interplay between developmental timing and environmental conditions governing kernel dehydration.

To characterize the genetic mechanisms of kernel dehydration, representative lines were selected from the KD RIL population, which exhibits diverse and distinct dehydration patterns, based on contrasting BLUP trajectories of KMC and KDR (Figure 1c,d). Figure 1c,d illustrate distinct phenotypic dehydration modes: (i) lines with similar initial KMC (34 DAP) but divergent final KMC (58 DAP); (ii) lines with divergent initial KMC converging to similar final moisture levels. Specifically, the phenotypic variation of kernel dehydration in this population is abundant, and we can clearly identify materials with different KDRs within the population, as reflected by the distinct dynamic changes of KMC during the dehydration process (34–58 DAP) (Figure 1c,d). Three-way ANOVA (Figure 1e) revealed that KMC variability was predominantly influenced by time (51.05% of the total variance), environment (33.03%), and genotype (1.8%), indicating high sensitivity of moisture loss to kernel development stage and environmental conditions, under which climatic factors vary. Given the substantial contribution of developmental stage and environment to KMC variation, we further performed two-way ANOVA (genotype × environment) for KMC across successive developmental stages to dissect how environmental effects differ as kernel development progresses. The results showed that the environmental effect on KMC was weak before 40 DAP but strong afterward (Figure S3), which is consistent with the known pattern that grain moisture is less affected by environment before physiological maturity and more influenced after physiological maturity (Gao et al., 2025). Additionally, we calculated the broad-sense heritability (H^2) of KMC at each time point, which ranged from 0.44 to 0.66 (Figure S4). These results are consistent with those reported by Li et al. regarding the primary roles of time and environment in shaping KMC variability (Li et al., 2021).

Identification of environmentally stable and pleiotropic QTLs for kernel dehydration traits

A total of 288 initial QTLs were detected across 5 field environments and the BLUP dataset, and intra-environment integration for KMC, KDR, and AUDDC generated 158 non-redundant QTLs (Figure 2a). Most of these QTLs showed strong environmental specificity, with only four KMC, three KDR, and six AUDDC QTLs identified in more than three environments, indicating that the majority of

© 2026 The Author(s).

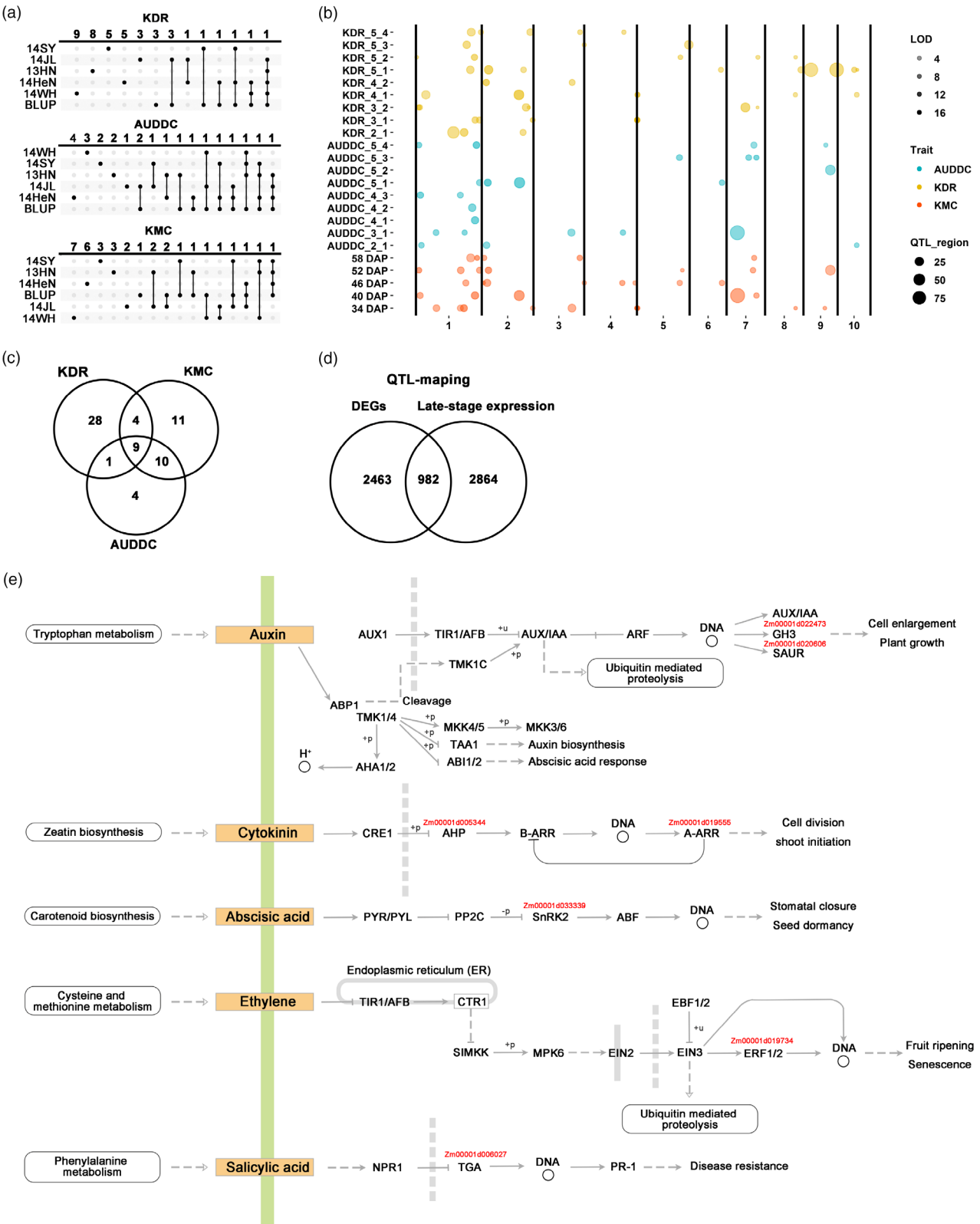

© 2026 The Author(s).

Figure 2. The genomic architecture and functional enrichment of dehydration-associated quantitative trait loci (QTLs).
(a) Environmental stability of QTLs visualized via UpSet plots: kernel moisture content (KMC): 54 initial loci (8 in 13HN, 8 in 14HeN, 9 in 14JL, 8 in 14SY, 10 in 14WH, 11 in best linear unbiased prediction [BLUP]); kernel dehydration rate (KDR): 57 loci (9 in 13HN, 10 in 14HeN, 8 in 14JL, 7 in 14SY, 12 in 14WH, 11 in BLUP); area under the dry-down curve (AUDDC): 47 loci (7 in 13HN, 12 in 14HeN, 7 in 14JL, 6 in 14SY, 5 in 14WH, 10 in BLUP).
(b) Chromosomal distribution of 100 consolidated QTLs: 42 KDR-related (yellow), 24 AUDDC-related (blue), 34 KMC-related (red). Density hotspots indicate trait-clustered regions.
(c) A Venn diagram of QTL overlap showing nine pleiotropic regions (shared across AUDDC/KDR/KMC) and trait-specific loci (AUDDC: 4, KDR: 28, KMC: 11).
(d) A Venn diagram intersecting DEGs within QTL intervals (left) and genes expressed in late-stage embryo/endosperm/seed (Chen et al., 2014).
(e) Kyoto Encyclopedia of Genes and Genomes (KEGG)-based phytohormone pathway mapping showing QTL-linked genes (shown in red font) involved in auxin, cytokinin, abscisic acid (ABA), ethylene, and salicylic acid metabolism.

dehydration-related QTLs are affected by environmental conditions (Figure 2a). We further performed cross-environment co-localization and integration of these loci, and finally obtained 100 non-redundant QTLs (KMC: 34, KDR: 42, AUDDC: 24) (Figure 2b; Tables S2 and S3). Given this strong environmental dependence, we subsequently focused on the subset of QTLs consistently detected across environments and on the high-confidence pleiotropic candidate regions shared among traits.

The 100 final non-redundant QTLs were distributed across all chromosomes, but mainly concentrated on Chr 1, 2, and 7. Notably, these QTLs tended to aggregate in the distal chromosomal regions rather than centromeric regions, indicating that the genetic loci associated with kernel dehydration traits exhibited a non-random distribution pattern. The phenotypic variation explained (PVE) by individual QTLs ranged from 4.53 to 27.37%, with the environmentally stable subset comprising one KMC QTL, two KDR QTLs, and four AUDDC QTLs (all detected in ≥3 environments) classified as major QTLs (PVE >10%), further underscoring their biological significance (Table S2). Notably, the consolidated interval qAUDDC1-2 identified herein fully covers *qKDR1* reported by Yu et al. (2025) using the same RIL population (Table S2), which cross-validates the robustness of our genome-wide QTL mapping workflow. While Yu et al. only characterized this individual locus, our work uncovers dozens of additional environment-stable and pleiotropic dehydration-associated loci across the maize genome (Yu et al., 2025).

Following the integration of environment-specific QTLs for KMC, KDR, and AUDDC (Figure 2b; Tables S2 and S3), we analyzed the combined set of 100 QTLs to identify genomic regions with pleiotropic effects. Although all three traits reflect aspects of kernel dehydration, they represent distinct physiological perspectives. Therefore, overlapping QTLs likely indicate coordinated genetic regulation rather than complete trait redundancy. Using a threshold of >50% genomic interval overlap, we identified 57 QTLs (57.1%) that were shared between at least 2 traits, underscoring substantial genetic coordination. The remaining QTLs included 4 unique to AUDDC, 28 to KDR, and 11 to KMC. The small proportion of AUDDC-specific QTLs (4/24) was due to its role as a comprehensive dehydration index closely correlated with KDR and KMC, while the higher proportions of unique QTLs for KDR (28/42) and KMC (11/34) resulted from their relative independence. In addition, nine high-confidence pleiotropic candidate regions were associated with all three traits (Figure 2c; Table S8), suggesting they act as genetic hubs for kernel moisture dynamics. We further validated these nine hub regions via multivariate QTL analysis (MT-MIM): seven were validated by multivariate QTL analysis (MT-MIM), with the MT-MIM LOD peaks falling within the original QTL intervals. The remaining two regions, while showing comparatively modest MT-MIM LOD signals, exhibited consistent cross-environment reproducibility in single-trait analyses (Figure S8; Table S8). Notably, these pleiotropic QTLs generally exhibited higher PVE and LOD scores than trait-specific ones, supporting their key regulatory roles. Thus, these nine high-confidence pleiotropic candidate regions represent critical regulatory regions for kernel dehydration.

In summary, we identified environmentally stable major QTLs and nine high-confidence pleiotropic candidate regions for maize kernel dehydration, providing a basis for dissecting kernel dehydration mechanisms.

RNA-seq-based identification of key phytohormone pathway genes associated with kernel dehydration via multi-source data integration

Kernel dehydration involves genes expressed in the late stages of kernel development, such as *RPG* (Yu et al., 2025). Thus, we performed RNA-seq on kernels of the inbred lines K22 and DAN340 at 30, 35, and 40 DAP to complement the QTL analysis and capture the gene expression dynamics during dehydration. A total of 9140 differentially expressed genes (DEGs) were identified, with 3445 localized within QTL intervals (AGPv4) (Figure S5). Building upon transcriptional dynamics reported by Chen et al. (2014), where late-stage expressed genes in the embryo are defined as those in co-expression modules C8–C12, late-stage expressed genes in the endosperm are those in modules C9–C14, and late-stage expressed genes in the whole seed are those in modules C7–C8, we identified a total of 10 146 late-development kernel-specific genes, among which 3846 genes were located within QTL intervals. Intersection of these datasets yielded 982 candidate genes (Figure 2d).

© 2026 The Author(s).

A Kyoto Encyclopedia of Genes and Genomes (KEGG) pathway analysis identified seven genes implicated in plant hormone signal transduction, including two auxin-related genes (*Zm00001d022473*, a putative indole-3-acetic acid-amido synthetase; *Zm00001d020606*, a SAUR-like auxin-responsive protein), two cytokinin-related genes (*Zm00001d005344*, a histidine-containing phosphor transfer protein; *Zm00001d019555*, a two-component response regulator), one ABA-related gene (*Zm00001d033339*, a serine/threonine-protein kinase belonging to subclass III SnRK2, is a key mediator of the ABA-SnRK2-bZIP signaling pathway that regulates maize kernel maturation and dehydration; Feng et al., 2022; Wang, Long, et al., 2025), one ethylene-related gene (*Zm00001d019734*, an ethylene-responsive transcription factor), and one salicylic acid-related gene (*Zm00001d006027*, a bZIP transcription factor family protein) (Figure 2e; Figure S6).

Collectively, by integrating DEGs, QTL-interval genes, and published late-stage transcriptional data, we were able to substantially narrow down the candidate genes. Through functional annotation analysis, we identified 7 genes out of the 982 candidate genes that are potentially involved in regulating grain desiccation via phytohormone signaling pathways. These findings verify the previously reported central role of hormone signaling in regulating kernel dehydration (Wang, Long, et al., 2025; Yu et al., 2025), providing high-confidence candidates for subsequent functional characterization and bridging transcriptional dynamics with QTL-derived loci to deepen understanding of dehydration mechanisms.

Candidate gene prioritization within integrated dehydration intervals

Using the B73 reference genome (AGPv4), we integrated our QTL intervals with the meta-QTL (MQTL) dataset from Wang et al. (2022). Since AUDDC serves as a comprehensive indicator of both KMC and KDR, this integration aligned with both traits in their study. For KDR and AUDDC specifically, the 42 KDR-related and 24 AUDDC-related QTLs were intersected with Wang et al.'s 11 mGdr loci (Wang et al., 2022), resulting in 5 QTLs spanning approximately 22.37 Mb—these shared loci represent conserved genomic regions associated with kernel dehydration that are consistently identified across independent studies (Figure 3a,c; Table S4). Likewise, for KMC and AUDDC, intersecting 34 KMC-related and 24 AUDDC-related QTLs with Wang et al.'s 34 mGwc loci identified 8 QTLs covering 30.45 Mb (Wang et al., 2022)—these overlapping regions denote robust genomic segments linked to kernel moisture characteristics, validated by their consistent detection across distinct genetic studies (Figure 3b,c; Table S4). These overlapping intervals represent high-confidence regions where genetic control of KDR and KMC converges across independent studies, strongly implicating them in core dehydration processes.

To further dissect the genetic basis of kernel dehydration and characterize the functional genes underlying these conserved MQTL intervals, we selected representative loci for in-depth validation and fine-mapping. Among the 13 conserved MQTL regions, KMC_2-1 was prioritized due to its reliable MQTL conservation and prominent genome-wide association studies (GWAS) signal associated with kernel moisture traits.

This QTL, KMC_21, spans a genomic interval of 12.4–15.5 Mb (Figure 3c), and its additive genetic effect is derived from the K22 haplotype. We performed progeny testing using selfed progeny of residual heterozygous line (RHL) KD071 (Figure S7A). We genotyped 113 segregating progeny with four KASP markers at chr2-13.194 Mb, chr2-13.884 Mb, chr2-13.187 Mb and chr2-13.193 Mb (Table S5), and classified them into two groups homozygous for the K22 haplotype and the DAN340 haplotype, respectively, based on marker genotypes within the KMC_2-1 interval.

Figure 3. Co-localization of quantitative trait loci (QTLs) with meta-QTLs and identification of key candidate genes for kernel dehydration.
(a, b) Chromosomal overlap analysis between newly mapped QTLs (orange) and Wang et al.'s meta-QTLs (purple) identified consensus intervals (red segments) for: kernel dehydration rate (KDR)-related loci (a): Intersection of 42 KDR/24 area under the dry-down curve (AUDDC) QTLs with 11 mGdr yielded five intervals (~22.37 Mb total); kernel moisture content (KMC)-related loci (b): Intersection of 34 KMC/24 AUDDC QTLs with 34 mGwc produced eight intervals (~30.45 Mb total).
(c) Characteristics of refined intervals: *x*-axis denotes interval names; bar heights indicate physical lengths (Mb); *y*-axis quantifies differentially expressed gene (DEG) counts per interval.
(d) KMC_2-1 interval (3.02 Mb): Top panel shows genome-wide association studies (GWAS) (14HeN_40 DAP, left axis) and QTL mapping (14SY_58 DAP, LOD = 3.3, right axis) with lead SNP chr2.S_13189074 ($P = 9.25 \times 10^{-8}$, red dot). The 100 kb region flanking the lead SNP contains four annotated genes (orange dots).
(e) Gene structures of the four genes within the 100 kb window; InDels are indicated by red arrows.
(f) Heatmap of expression levels for the four genes across kernel developmental stages (30, 35, and 40 DAP), with $\log_{10}$ (FPKM + 1) transformed values.
(g) Expression divergence driven by promoter InDel: *T*-test significance; *** indicates $P < 0.001$ for 14HeN_58DAP, ** indicates $P < 0.01$ for 14HeN_AUDDC_5_4.
(h) Phylogenetic tree of *Zm00001d002455* homologs in rice and Arabidopsis.
(i) KMC_2-2 interval (0.70 Mb): QTL mapping (BLUP_34 DAP, LOD = 3.5; 14HeN_34 DAP, LOD = 3.4) with gene annotations: variants (orange, 18/21) and DEGs (red, 7/18), including *Zm00001d005798*.
(j) Gene structure of *Zm00001d005798*, with red arrows indicating 14 InDels within its genomic region and adjacent 1-kb upstream/downstream regions.
(k) Heatmap of *Zm00001d005798* expression across developmental stages (30/35/40 DAP), with $\log_{10}$ (FPKM + 1) transformed values.
(l) Phylogenetic tree of *Zm00001d005798* homologs in rice and Arabidopsis.

© 2026 The Author(s).

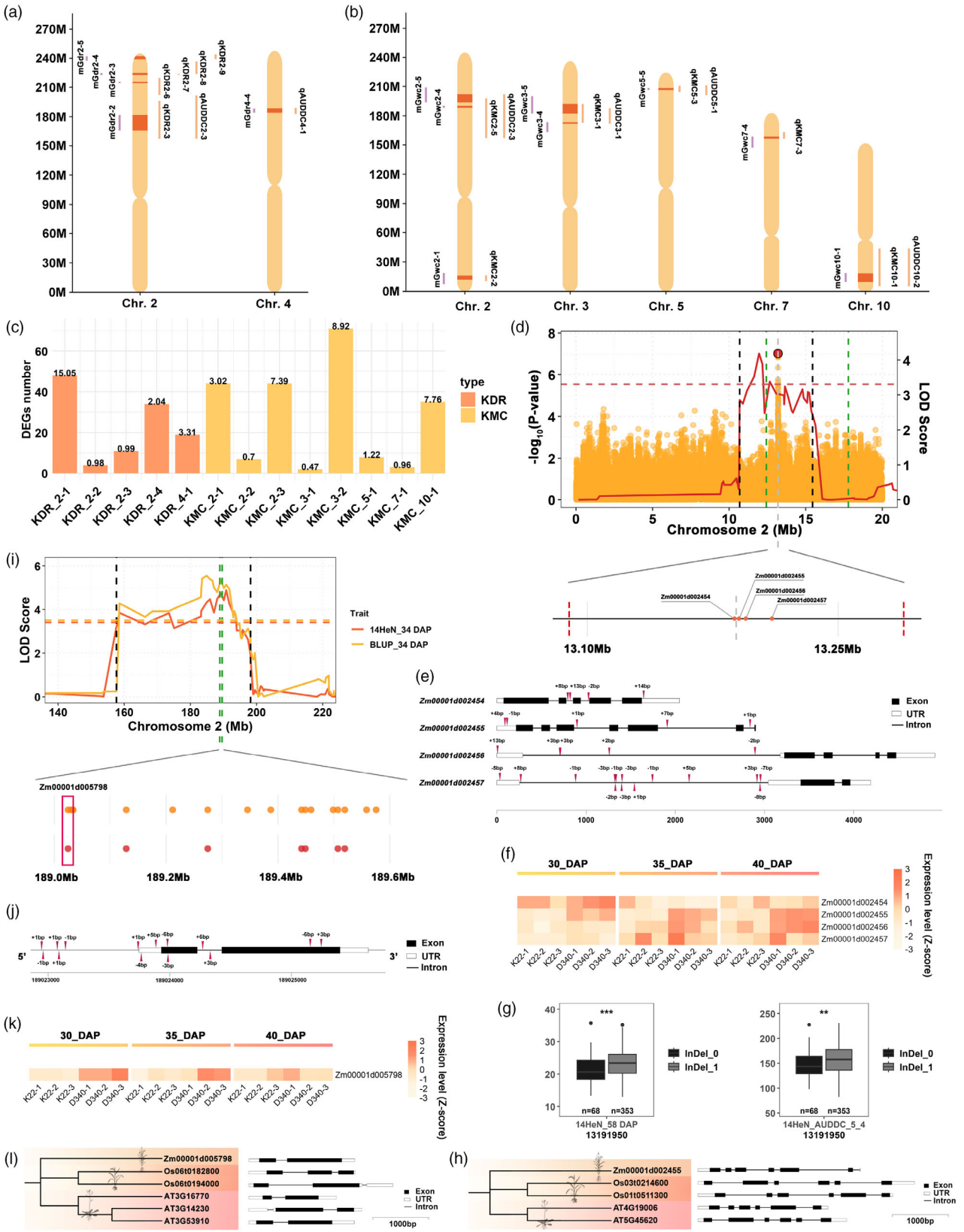

© 2026 The Author(s).
The Plant Journal published by Society for Experimental Biology and John Wiley & Sons Ltd.,

We compared KMC phenotypes of the two groups at 49 and 54 DAP. At 49 DAP, no significant difference in KMC was observed between homozygous DAN340 and K22 progeny. At 54 DAP, DAN340-type lines exhibited significantly lower KMC than K22 homozygotes, with a mean reduction of 4.40 percentage points. Overall, progeny carrying DAN340 alleles showed accelerated moisture loss and lower late-stage kernel moisture (Figure S7B).

To identify candidate genes within this functionally validated interval, we performed fine-mapping integrating GWAS, parental variant calling, and RNA-seq analysis. This interval harbors a highly significant nonsynonymous SNP (chr2.S_13189074, $P = 9.25 \times 10^{-8}$) identified through association analysis (Figure 3d). The 100 kb region flanking this SNP contains only four annotated genes (Figure 3d); although all four harbor InDels/SVs between the parental lines, none of these variants reside in coding sequences—they are confined to UTRs or introns (Figure 3e). RNA-seq analysis revealed that among these four genes, only *Zm00001d002455* is differentially expressed, and it is located merely 37 bp from the lead SNP. *Zm00001d002455* harbors five variation sites, including a critical +1-bp InDel in the intron closest to the promoter region (Figure 3d–g). Significantly, this +1-bp InDel drives differential expression, with *t*-tests confirming genotype-dependent expression divergence in key kernel moisture-related traits (e.g., 14HeN_58DAP and 14HeN_AUDDC_5_4; $P < 0.05$) (Figure 3g; Tables S6 and S7). Notably, *Zm00001d002455* encodes a 26S proteasome regulatory subunit homolog predicted to contain a single PINT domain. Furthermore, independent public kernel transcriptome datasets demonstrate that this gene exhibits a consistent trend of elevated expression during late kernel developmental stages in B73 embryo and endosperm (Chen et al., 2014). Furthermore, its homologs in Arabidopsis and rice encode the 26S proteasome subunit RPN9, which has been hypothesized to regulate vascular system development by degrading a series of proteins (Jin et al., 2006; Lin et al., 2024; Pan & Tang, 2018; Shibahara et al., 2002) (Figure 3h). Therefore, the convergence of promoter/genic variation, physical proximity to the lead SNP, differential expression, domain architecture, and plausible biological function strongly nominates *Zm00001d002455* as a top prioritized candidate gene underlying this major KMC locus.

Similarly, the KMC_2-2 interval, which overlaps qKMC_2-5 and mGwc2-4 and spans 0.70 Mb, encompassing 21 genes, was examined closely (Table S4). Variant screening revealed 18 genes harboring or proximal to InDel/SV sites between parental lines K22 and DAN340. Subsequent RNA-seq identified 7 DEGs from these 18 candidates (Figure 3j). Among the 7 DEGs, *Zm00001d005798* was prioritized for functional validation (Figure 3l) based on its annotation as an ethylene-responsive transcription factor, RAP2-2, and public time-resolved kernel omics datasets reveal that this gene displays elevated expression trends at late kernel developmental stages in B73 endosperm (Chen et al., 2014). Notably, *Zm00001d005798* is located within these nine high-confidence pleiotropic candidate regions, further supporting the gene association with kernel dehydration traits. Structural analysis identified 14 InDels in its genomic region and the adjacent 1-kb upstream and downstream regions (Figure 3k). Protein domain prediction further confirmed the presence of a single AP2 domain. Its rice homologs include *Os03g0182800*, which regulates endosperm starch/protein synthesis (affecting chalkiness), ethylene signaling, and development, with its loss enhancing stress tolerance (Hu et al., 2025; Yang et al., 2002; Zhang, Li, et al., 2020); and Os06g0194000, which promotes drought tolerance via ABA signaling and proline biosynthesis (Li et al., 2018) (Figure 3l). Arabidopsis homologs (*AT1G53910*, *AT3G14230*, *AT3G16770*) inhibit ethylene-regulated seed dormancy via the N-degron pathway and hormone crosstalk (Bissoli et al., 2025; Wang, Gomes, et al., 2021) (Figure 3l). The conserved function of its homologs across species suggests *Zm00001d005798* is a prioritized candidate gene modulating maize kernel dehydration dynamics.

DISCUSSION

Maize, a globally pivotal cereal crop with significant economic and nutritional value, achieved a global annual output of 1.22 billion metric tons in 2024 (https://www.fao.org/). However, maize cultivars with low KMC at harvest are scarce in China and most other countries, which has severely impeded the popularization of mechanical harvesting and increased the costs of post-harvest drying and storage. Thus, elucidating the molecular mechanisms regulating KMC is essential for breeding low KMC maize varieties.

Phenotypic variation and environmental impact of kernel dehydration

The exact time of physiological maturity cannot be precisely determined due to the combined effects of environmental factors and genetic backgrounds (Afuakwa & Crookston, 1984; Jin et al., 2002). We therefore conducted repeated measurements of KMC for each line starting at 34 DAP with a 5-day interval, to systematically characterize the dynamic changes in kernel moisture during kernel development (Li et al., 2021). KMC was measured directly and continuously using a BLD5604 hygrometer, a method that reduces field workload and saves time and labor; however, it is susceptible to the inherent developmental status of kernels, underscoring the need to develop simpler and more efficient KMC measurement methods and instruments. We collected KMC data from five locations (Table S1), with the lowest KMC detected in 14WH, a phenomenon we attribute to the high temperatures in that

© 2026 The Author(s).

growing season (Figure 1b). Notably, dissecting kernel dehydration dynamics cannot rely solely on harvest-stage KMC. Actually, multi-stage measurements and integrated analysis of three core traits are indispensable: KMC, which reflects moisture status at specific developmental stages; KDR, which captures the dynamic rate of moisture loss; and AUDDC, which integrates the overall dehydration process (Jia et al., 2020; Li et al., 2021; Yang et al., 2010).

Although parental lines K22 and DAN340 showed no significant phenotypic differences under some environmental conditions and exhibited relatively slow dehydration rates across all environments, their progeny (the KD RIL population) displayed substantial phenotypic variation. This finding was critical for the successful identification of multiple QTLs associated with KMC, KDR, and AUDDC, and it also underscored that the detection of abundant QTLs does not depend on obvious parental trait divergence, thereby providing great potential for mining favorable alleles to guide the breeding of fast-dehydrating maize hybrids. Notably, the distinct kernel moisture dynamic trajectories of representative RILs visualized in Figure 1c,d are plotted using BLUP values integrated across all five tested environments. The BLUP approach largely removes confounding environmental fluctuation and genotype-by-environment interaction effects from phenotypic datasets; therefore, the consistent divergence in dehydration patterns among different RIL genotypes observed in these curves is driven predominantly by intrinsic genetic variation within the KD RIL population rather than external environmental factors. We selected two representative contrasting lines, KD113 and KD012, to dissect the genetic origin of this phenotypic separation. These two lines possess nearly equivalent initial KMC at 34 DAP but exhibit markedly different moisture loss magnitudes at late kernel developmental stages. We further compared the full allelic genotypes of KD113 and KD012 across all QTL intervals detected using BLUP phenotypic data. In the majority of genomic regions associated with kernel dehydration on chromosomes 1, 2, 3, 7, and 10, KD113 and KD012 harbor divergent homozygous haplotypes, and only a small fraction of these QTL intervals carry identical genotypes between the two lines. These stable, fixed genotypic differences across dehydration-regulating loci establish the fundamental genetic basis for their permanently divergent kernel dehydration performance.

A three-way ANOVA revealed that the proportion of genotype (G) was relatively low across the entire kernel developmental period (Figure 1e). However, a two-way ANOVA (genotype × environment) performed at individual time points showed that G accounted for a large proportion before 40 DAP and then showed a decreasing trend thereafter (Figure S3) (Gao et al., 2025). This result is consistent with previous findings that kernel dehydration is less affected by the environment in the early stage but more profoundly influenced in the late stage (Liu et al., 2020). We also calculated the broad-sense heritability (H^2) at each time point, with the maximum value only reaching 0.66 (Figure S4), which was lower than that reported in a prior study (Li et al., 2021). This discrepancy may be attributed to the significant effect of the environment on physiological maturity. Collectively, these results indicate that mining of QTLs and genes related to kernel dehydration in maize is a complex task that requires greater research efforts and investment.

Genetic architecture of kernel dehydration: environmentally stable and pleiotropic QTLs

In this study, we determined the KMC, KDR, and AUDDC of the KD RIL population (K22 and DAN340) at the late stage of kernel development through multi-year and multi-location analysis. Since KMC was measured continuously at multiple developmental stages, multiple traits were obtained, and the continuous dynamic changes of these traits could also be observed. Combined with genotypic data, QTL localization analysis was performed. Although a total of 100 QTLs were identified, most were detected in only 1 or 2 environments, indicating strong environmental sensitivity; however, 13 QTLs consistently detected across three or more environments and 9 high-confidence pleiotropic candidate regions shared among all 3 traits emerged as the most robust findings. The average PVE of individual QTLs was approximately 8.75%, indicating that grain moisture is controlled by many loci with minor effects. Notably, 21 QTLs had a phenotypic contribution rate exceeding 10%, and 9 QTL regions were mapped for all three traits. Consistent with our QTL mapping results, the *qKDR1* locus functionally dissected by Yu et al. (2025) is embedded within our qAUDDC1-2 interval, which demonstrates the accuracy of our multi-trait, cross-environment mapping strategy (Yu et al., 2025). Their single-locus functional analysis complements the broad genetic architecture uncovered in the present research.

We acknowledge that KMC, KDR, and AUDDC are mathematically inter-related derived traits. Although 150 trait datasets were subjected to QTL scanning, estimation of the effective number of independent tests suggested that the true number of independent genetic signals ranged from 16 to 36, which greatly reduces the overall multiple-testing burden relative to the nominal 150 independent tests. This mathematical inter-relatedness may lead to some degree of QTL overlap that reflects statistical correlation rather than genuine biological pleiotropy. To address this concern, we performed multivariate QTL analysis using MT-MIM specifically on the nine candidate regions (Joehanes & Nelson, 2008). This analysis confirmed seven of the nine regions, with the MT-MIM LOD peaks located within the original QTL intervals (Figure S8). For the remaining two regions, the MT-MIM signals were

© 2026 The Author(s).

comparatively modest (Figure S8); however, both exhibited consistent cross-environment reproducibility in single-trait analyses, suggesting that they remain plausible candidate loci. Notably, the MT-MIM analysis was performed as a supportive validation strategy, while our primary conclusions are based on the single-trait QTL mapping results, for which permutation-based significance thresholds were rigorously established. Therefore, we have refrained from referring to these nine regions as definitive pleiotropic loci and instead describe them as high-confidence pleiotropic candidate regions, emphasizing that functional validation will be required to definitively confirm their biological roles.

To further explore the molecular basis behind these QTL signals, we integrated RNA-seq data and a previously published transcriptomic dataset (Chen et al., 2014) and identified 982 genes that were differentially expressed between the two parental lines during late kernel development and that resided within these 100 QTL intervals. KEGG analysis of the 982 high-confidence candidate genes identified a set of candidate genes involved in plant hormone signal transduction that may regulate kernel dehydration during the late developmental stage. For instance, *Zm00001d033339* acts as a core component regulating kernel maturation in the maize ABA signaling pathway; it exhibits functional redundancy with other subclass III SnRK2s and mediates the conserved ABA-SnRK2-bZIP signaling pathway, and its loss of function leads to delayed kernel maturation and impaired dehydration (Feng et al., 2022; Wang, Long, et al., 2025).

Candidate genes and conserved regulatory mechanisms

The intersection of our QTLs with MQTLs identified 13 high-confidence conserved genomic regions (Wang et al., 2022), from which 2 candidate genes—*Zm00001d002455* and *Zm00001d005798*—emerged as putative regulators of maize kernel dehydration based on genetic and transcriptomic evidence. Notably, our RNA-seq profiling was limited to the 30–40 DAP window and cannot provide transcriptional evidence for late kernel developmental stages. Instead, two independent published time-series kernel transcriptome datasets consistently reveal that both *Zm00001d002455* and *Zm00001d005798* have a tendency toward higher expression during late seed maturation, which provides indirect transcriptional support for their regulatory roles in kernel dehydration.

The candidate gene *Zm00001d002455* is annotated as 26S proteasome non-ATPase regulatory subunit 13 homolog A, and its homologs in both *Arabidopsis thaliana* and *Oryza sativa* encode RPN9, a core subunit of the 19S regulatory particle (RP) within the 26S proteasome (Miller & Gordon, 2005; Pan & Tang, 2018). The lid, composed of eight non-ATPase subunits including RPN9, is primarily responsible for recognizing ubiquitinated substrates and cleaving the ubiquitin chain (deubiquitination) prior to substrate degradation and translocation into the 20S core (Pan & Tang, 2018). Notably, studies in *Nicotiana benthamiana* have suggested that RPN9 may play a role in vascular development. Downregulation of RPN9 led to altered vascular patterning, possibly through its effects on auxin transport and brassinosteroid signaling (Jin et al., 2006). This observation is particularly relevant to kernel dehydration, as the vascular system, especially the bundles connecting the stem to the panicle, serves as the primary conduit for water transport to and from the developing grain (Li et al., 2017). In cereals, it has been proposed that excess water entering the grain during filling, as well as water lost during maturation drying, is effluxed through the xylem of these vascular bundles (Liu et al., 2017). It is therefore plausible that *Zm00001d002455* contributes to variation in maize KDRs by influencing the development or functional properties of these vascular connections. Altered RPN9 expression could potentially impact the efficiency of water movement through the pedicel or cob, thereby affecting the rate of moisture loss during the final stages of grain maturation. This hypothesis provides a potential link between the molecular function of a proteasome subunit and a complex agronomic trait, warranting further investigation. We note the limitation of our current experimental evidence for *Zm00001d002455*. We only validated the overall genetic effect of the KMC_2-1 interval via progeny testing of RHL KD071. Although this assay confirmed that the interval carries functional variants affecting late-stage kernel dehydration, the 3.02-Mb segment contains multiple annotated genes, making it impossible to attribute the observed phenotypic difference solely to *Zm00001d002455*. The effect detected at 54 DAP may reflect the combined action of several linked loci. Thus, *Zm00001d002455* currently represents a prioritized candidate.

The AP2/ERF family, the largest plant-specific transcription factor group, is extensively involved in growth, development, and stress responses (Fukao et al., 2006; Park et al., 2001; Qi et al., 2023). The ERF subfamily, its major component, serves as a key downstream regulator of ethylene signaling and contains a conserved AP2 domain (Cheng et al., 2023; Müller & Munné-Bosch, 2015; Sakuma et al., 2002; Xu et al., 2011). The candidate gene *Zm00001d005798* (encoding RAP2-2), located within nine high-confidence pleiotropic candidate regions, belongs to the ERF subfamily and is involved in biotic stress responses and heat-induced leaf senescence (Cheng et al., 2023; Han et al., 2023; Qi et al., 2023). Its rice homolog *Os03g0182800* regulates endosperm starch and protein synthesis, influencing chalkiness formation, and participates in ethylene signaling during seed maturation and aboveground development. Its deletion enhances seed germination under waterlogging and drought stress tolerance

© 2026 The Author(s).

(Hu et al., 2025; Yang et al., 2002; Zhang, Li, et al., 2020). Another homolog, *Os06g0194000*, contributes to drought tolerance by upregulating ABA signaling and proline biosynthesis genes under stress (Li et al., 2018). In Arabidopsis, homologs *AT1G53910*, *AT3G14230*, and *AT3G16770* act as core repressors of ethylene-mediated seed dormancy, integrating ethylene, cold, and GA/ABA signals via the N-degron pathway (Bissoli et al., 2025; Wang, Gomes, et al., 2021). In maize, kernel dehydration is coordinately regulated by ethylene and ABA signaling: microRPG1 delays dehydration by inhibiting ethylene-responsive factors, while ABA promotes maturation drying via the SnRK2-bZIP module (Wang, Long, et al., 2025; Yu et al., 2025). Additionally, KDR and dehydration conditions affect seed germination rate and vitality (Fan et al., 2014; Kovach & Bradford, 1992). Collectively, these findings suggest that *Zm00001d005798*, as an ERF subfamily member involved in ethylene signaling and stress responses, and with homologous genes related to seed maturation, stress tolerance, and hormone pathway crosstalk, is a potential candidate gene regulating maize kernel dehydration.

Collectively, integration of MQTL mapping, transcriptomic profiling, and cross-species homologous evidence delivers indirect multi-omics evidence to treat *Zm00001d002455* and *Zm00001d005798* as high-confidence prioritized candidates. Their association with conserved dehydration-related QTLs and genotype-dependent expression patterns, combined with the established roles of their homologs in vascular development, seed maturation, and hormone signaling, strengthens their candidacy. We acknowledge the limitations of our current candidate gene screening workflow, which relies primarily on DEGs and non-coding structural variants (SVs) without systematically scanning coding-region mutations capable of altering amino acid sequences and protein tertiary structures. This screening bias may overlook causal genes whose protein conformational changes drive trait variation in the absence of obvious expression shifts. Nevertheless, definitive confirmation of their causative roles requires direct functional validation. To this end, we are currently employing reverse genetic approaches, including CRISPR-Cas9-mediated knockout and overexpression, to characterize their effects on KMC, KDR, and AUDDC across multiple environments. These ongoing efforts will ultimately elucidate the molecular mechanisms by which these genes govern this complex agronomic trait.

MATERIALS AND METHODS

Plant materials and field planting

The two parental lines of the maize RIL population are the domestic elite inbred lines named DAN340 and K22 in the current study, and there are a total of 199 RILs. The KMC of DAN340 and K22 was low. The field tests were repeated twice. In the summer of 2013, 199 RILs were planted in Hainan (13HN; Sanya, Hainan, E 109°51′, N 18°25′). In the summer of 2014, 199 RILs were planted in Henan (14HeN; Xinxiang, Henan, E 113°91′, N 35°31′), Jilin (14JL; Gongzhuling, Jilin, E 124°69′, N 43°79′), Liaoning (14SY; Shenyang, Liaoning, E 123°43′, N 41°81′), and Hubei (14WH; Wuhan, Hubei, E 114°32′, N 30°58′). These five locations basically cover the main maize planting areas in China and have environmental representativeness.

In this experiment, a randomized plot design was adopted for each of the two field trials to conduct the initial QTL mapping. For each population, two replicates were set up in each environment. Each RIL was planted in one row, and the distance between two adjacent plants was 0.025 m; the row spacing was designed according to the optimal row spacing for the planting environment (ranging from 50 to 70 cm).

Phenotypic data collection and statistical analysis

In order to accurately display the dynamic changes of KMC during the entire kernel development, we recorded the pollination date of each line. We used GE's BLD5604 moisture meter to measure the transient KMC at each location every 6 days for a total of five successive stages—34, 40, 46, 52, and 58 days after pollination (DAP) (Table S1). For each line, 5 individuals were each measured twice, and the average of these 10 moisture readings was recorded as the line's KMC value. The KDR was derived between sequential time intervals by applying the following formula:

$$\mathrm{KDR}_k_s = [(\mathrm{KMC}_n - \mathrm{KMC}_{n+1})/6] \times 100\%$$

where $s < k$ and s, $k \in \{1, 2, 3, 4, 5\}$, and n is the number of environments. Therefore, 10 KDR traits were obtained based on measurements at 5 time points: 34–40 DAP (KDR_2_1), 40–46 DAP (KDR_3_2), 46–52 DAP (KDR_4_3), 52–58 DAP (KDR_5_4), 34–46 DAP (KDR_3_1), 40–52 DAP (KDR_4_2), 46–58 DAP (KDR_5_3), 34–52 DAP (KDR_4_1), 40–58 DAP (KDR_5_2), and 34–58 DAP (KDR_5_1).

In addition, we used the AUDDC to efficiently quantify the dehydration rate (Yang et al., 2010). The formula used to calculate AUDDC is:

$$\mathrm{AUDDC}_k_s = \sum_{i}^{n-1} \left[(\gamma_i + \gamma_{i+1})/2\right](t_{i+1} - t_i)$$

where $s < k$ and s, $k \in \{1, 2, 3, 4, 5\}$, and $t_i \in \{34, 40, 46, 52, 58\}$ where γ is the converted meter reading, *ith* is the measured time, and t_i is the corresponding DAP. Therefore, 10 AUDDC traits were obtained based on measurements at 5 time points: 34–40 DAP (AUDDC_2_1), 40–46 DAP (AUDDC_3_2), 46–52 DAP (AUDDC_4_3), 52–58 DAP (AUDDC_5_4), 34–46 DAP (AUDDC_3_1), 40–52 DAP (AUDDC_4_2), 46–58 DAP (AUDDC_5_3), 34–52 DAP (AUDDC_4_1), 40–58 DAP (AUDDC_5_2), and 34–58 DAP (AUDDC_5_1).

For each stage, KMC, KDR, and AUDDC data reflected the location that was regarded as the environmental factor. A mixed linear model was constructed, treating the intercept as the fixed effect and genotype and environment as random effects. The variance components of genotype and environment were estimated based on restricted maximum likelihood (REML) using the R package 'lme4' (Null et al., 2011). The BLUP value for each line was obtained. We conducted a three-way ANOVA and time-point-specific two-way ANOVAs to dissect phenotypic variation sources. The broad-sense heritability (H^2) was calculated as follows (Knapp et al., 1985):

$$H^2 = \sigma_g^2 / \left(\sigma_g^2 + \frac{\sigma_{ge}^2}{n} + \frac{\sigma_e^2}{nr} \right)$$

© 2026 The Author(s).

where σ_g^2 represents the genotypic variance, σ_{ge}^2 represents the genotype × environment variance, σ_e^2 represents the residual error variance, and n and r are, respectively, the mean number of environments ($n = 5$) and replications ($r = 2$) that combine location and years as a random effect. In total, this experimental design yielded 150 kernel moisture-related traits: 30 KMC traits (5 time points × 6 datasets), 60 KDR traits (10 intervals × 6 datasets), and 60 AUDDC traits (10 intervals × 6 datasets). All data from five environments and BLUP were used for subsequent analyses, including 30 KMC traits, 60 KDR traits, and 60 AUDDC traits (Table S1).

QTL analysis

The QTL analysis was performed using a population of RILs derived from [K22 × DAN340]. The genetic linkage map used was derived from references (de Givry et al., 2005; Ganal et al., 2011; Kosambi, 2011). The total genetic distance was 1698.4 cM with an average of 0.81 cM between adjacent markers. This dense map provides a robust framework for precise QTL localization.

QTL mapping was performed using the composite interval mapping (CIM) method implemented in Windows QTL Cartographer V2.5 software (Zeng, 1994). Analyses were conducted separately for the raw phenotypic data (KMC at each time point, KDR, AUDDC) from each of the five environments and the across-environment BLUP values. For CIM, a walk speed of 0.5 cM and a model 6 (Zmap) window size of 10 cM were used. The genome-wide significance threshold for declaring a putative QTL was determined for each trait (both raw and BLUP) by performing 1000 permutations at a significance level of $P = 0.05$, which established the minimum logarithm of odds (LOD) score required. QTLs exceeding this permutation-derived threshold were considered significant. The 95% confidence interval for each QTL was defined as the interval spanning two LOD units down from the peak LOD position. Additionally, QTLs explaining ≥10% of the phenotypic variance (R^2) were classified as major QTLs. The initial QTL mapping was based on the B73 reference genome (AGPv2). To ensure the accuracy of subsequent data integration, the obtained QTL intervals (spanning 10 chromosomes with a total length of 689.964 Mb) were converted to the coordinate system of the B73 reference genome (AGPv4).

To assess the family-wise multiple testing burden across all 150 kernel dehydration-related traits, the effective number of independent tests (M_{eff}) was computed from the phenotypic correlation matrix. Two complementary approaches were implemented: the eigenvalue-based method Li and Ji (2005), and a PCA-based approximation counting the number of principal components explaining ≥90% of total phenotypic variance. The nominal total number of traits was 150; M_{eff} was estimated as 36 by the Li & Ji method and 16 via the PCA 90% criterion (Li & Ji, 2005). Per-trait permutation-derived LOD thresholds were retained for QTL identification, while M_{eff} values were used to evaluate global false positive risk across all scans.

To further evaluate whether the nine candidate regions represent genuine pleiotropic loci, we performed a supportive multivariate QTL analysis using multiple-trait multiple-interval mapping (MT-MIM) implemented in QGene 4.4.0 (Joehanes & Nelson, 2008). For each of the nine regions, we selected three representative traits (one KMC trait, one KDR trait, and one AUDDC trait) with the highest LOD scores from the univariate scans within each category. Multivariate scans were conducted with a walk speed of 0.1 cM across each chromosome interval. A detailed summary of the trait combinations and MT-MIM results is provided in Figure S8.

Genome-wide association analysis

GWAS for 150 kernel moisture-related traits were performed using the compressed mixed linear model in TASSEL V5.0 (Bradbury et al., 2007; Zhang et al., 2010). The phenotypic data for these traits have been previously published in Li et al. (2021). Analyses utilized 11.21 million high-quality SNPs, ~2.02 million InDels, and ~274 600 common SVs (all with MAF >5%) from the pan-Zea genetic variation map (Gui et al., 2022), with these variants—particularly InDels and SVs—used to analyze genetic differences between the parental lines K22 and DAN340. The mixed linear model controlled for population structure (Q-matrix) and kinship (K-matrix) to test the significance of genome-wide SNP-trait associations (Gui et al., 2022; Yang et al., 2014). The most significant SNPs were distributed within genes or in intergenic regions, so the genes closest to the most significant SNPs (including the genes where the SNPs were located within genes and the nearest genes in the intergenic regions) were identified as the most likely candidate genes. Candidate gene annotations were based on MaizeGDB (http://www.maizeGDB.org) and Gramene (http://ensembl.gramene.org/Zea_mays/Info/Index).

RNA-seq and data analysis

The two parental lines of the RIL population, DAN340 and K22, were used for this analysis. The kernels of these inbred lines were sampled by manual dissection at 30, 35, and 40 DAP in 2025 (Sanya, Hainan, E 109°51′, N 18°25′), frozen immediately in liquid nitrogen, and stored at −80°C. For each inbred line and at each time point (DAP), kernels were harvested from nine individual plants. These kernels were then randomly combined into three groups, with each group consisting of a pooled sample from three plants. Each pooled sample constituted one biological replicate, resulting in three biological replicates per inbred line per time point. Total RNA was isolated from the seed using a Quick RNA Isolation Kit (Huayueyang, Beijing, China) according to the manufacturer's instructions. The stranded RNA libraries were constructed using the VAHTS Universal V8 RNA-seq Library Prep Kit for MGI (Vazyme, Nanjing, China) following the manufacturer's recommendations. After library preparation, QC, and pooling, paired-end sequencing was performed on the DNBSEQ-T7 (MGI, Shenzhen, China) at the Sequencing Platform of the National Key Laboratory of Crop Genetic Improvement in Huazhong Agricultural University (Wuhan, China).

Raw paired-end reads were quality-filtered using fastp and aligned to the maize B73 reference genome (RefGen_v4; http://ftp.ensemblgenomes.org/pub/plants/release-41/fasta/zea_mays/dna) sequence assembly with HISAT 2.2.1 (Kim et al., 2015). Gene expression was quantified as fragments per kilobase of transcript per million mapped reads (FPKM) using featureCounts (Liao et al., 2014) from the Subread package. DEGs between genotypes were identified using DESeq2 software, with an adjusted P-value threshold of <0.01 and a fold change ≥2. KEGG pathway enrichment analyses were performed using the KOBAS-i web server (http://bioinfo.org/kobas/) (Bu et al., 2021).

Candidate gene systematic analysis

To further investigate the potential function of the candidate genes identified through QTL mapping and GWAS, a systematic *in silico* analysis was conducted. The amino acid sequences of the candidate genes were retrieved from the Gramene database (http://www.gramene.org/). Protein domain architectures were predicted using the SMART online tool (http://smart.embl.de/). To elucidate evolutionary relationships, orthologous genes of the

© 2026 The Author(s).

candidate genes were identified and their amino acid sequences were downloaded from Gramene for *A. thaliana* L., *Oryza sativa* L. ssp. *indica*, and *Oryza sativa* L. ssp. *japonica*. Multiple sequence alignment was performed using the MUSCLE algorithm within MEGA X software (Kumar et al., 2018). A neighbor-joining phylogenetic tree was constructed based on the aligned sequences using the maximum likelihood method in MEGA, with branch support assessed by 1000 bootstrap replicates (Kumar et al., 2018). Concurrently, gene expression patterns of the candidate genes were analyzed using RNA-seq data from the parental lines. For visualization, gene expression values were $\log_{10}$-transformed (FPKM + 1) to normalize dynamic range and address zero values, then row-standardized to *Z*-scores across samples.

Residual heterozygous line progeny validation of the KMC_2-1 QTL interval

Genotypic and phenotypic assays were performed to verify the genetic effect of the KMC_2-1 QTL interval. The RHL KD071 from the KD RIL population was selected for this experiment, as it harbors a heterozygous chromosomal segment spanning 12 177 121–15 639 111 bp on chromosome 2 that fully covers the target interval of KMC_2-1 (12 427 429–15 447 887 bp). Four KASP markers spanning the KMC_2-1 interval were developed to genotype self-pollinated progenies derived from KD071. Based on marker genotypes within this target segment, all segregating progenies were categorized into two groups carrying interval-homozygous K22 and DAN340 haplotypes, respectively. Two-sample Student's *t*-tests were implemented to compare kernel moisture and dehydration-related traits between the two homozygous haplotype groups, thereby validating the regulatory effect of this genomic segment on KMC. Primer sequences of the four KASP markers are provided in Table S5.

ACKNOWLEDGEMENTS

This work was supported by the National Key Research and Development Program of China (2023YFD1200501), the National Natural Science Foundation of China (32201851), and the Fundamental Research Funds for the Central Universities (2662023ZKQ001).

Generative AI tools were used for partial English-language polishing and grammatical refinement of selected sections of the manuscript. All experimental design, raw data acquisition, data analysis, scientific interpretation, and core manuscript writing were completed entirely by the authors. All AI-processed texts have been comprehensively reviewed, revised, and verified by all authors to guarantee the accuracy of experimental facts, citations, and scientific conclusions. No generative AI tools were used to generate experimental data, figures, or original research findings.

AUTHOR CONTRIBUTIONS

DY: Writing—original draft, visualization, validation, methodology, investigation, formal analysis, data curation, conceptualization. HW: Investigation, data curation. YP: Investigation. YL: Investigation. YX: Investigation. LZ: Investigation. LW: Investigation. JZ: Writing—review and editing. YX: Supervision, methodology. JY: Supervision, conceptualization. WL: Writing—review and editing, supervision, project administration, funding acquisition, conceptualization.

CONFLICT OF INTEREST

The authors declare no competing interests.

DATA AVAILABILITY STATEMENT

All data supporting the findings of this study are available within the manuscript and its supplementary materials. Raw RNA-seq sequencing data generated in this study are publicly available in the NCBI Sequence Read Archive (SRA) under BioProject accession PRJNA1510314.

SUPPORTING INFORMATION

Additional Supporting Information may be found in the online version of this article.

Figure S1. Moisture content dynamics of parental lines (DAN340 and K22) across different environments.

Figure S2. Phenotypic distribution of all traits relevant to KMC, AUDDC, and KDR in KD RIL (A-13HN, B-14HeN, C-14JL, D-14SY, E-14WH, F-BLUP).

Figure S3. Variance partitioning via time-point-specific two-way ANOVA, showing the proportions of KMC phenotypic variation components (genotype [G], environment [E], G × E interaction) at each measurement time point.

Figure S4. Broad-sense heritability (H^2) of KMC at each time point (34 DAP, 40 DAP, 46 DAP, 52 DAP, 58 DAP).

Figure S5. Temporal dynamics of differentially expressed genes (DEGs) during kernel dehydration.

Figure S6. Expression profiles of hormone pathway candidate genes.

Figure S7. Verification of the genetic effect of major kernel moisture content QTL KMC_2-1 using segregating progenies derived from residual heterozygous line KD071.

Figure S8. Multi-trait joint QTL analysis of the nine high-confidence pleiotropic candidate regions for maize kernel dehydration-related traits performed in QGene 4.4.0.

Table S1. Basic statistics of KMC, AUDDC, and KDR in KD RIL.

Table S2. Summary of 100 consolidated QTLs for dehydration traits (AGPv2 coordinates).

Table S3. Composition of consolidated QTL intervals.

Table S4. Meta-QTL validated intervals (AGPv4 coordinates).

Table S5. KASP primer sequences used for the fine mapping of the KMC_2-1.

Table S6. Phenotypic data of the KD RIL population for all 150 kernel dehydration-related traits (KMC, KDR, AUDDC).

Table S7. Kernel phenotypic data of the AMP association panel collected at 14HeN_46 DAP.

Table S8. Summary of the nine high-confidence pleiotropic candidate genomic regions associated with KMC, KDR, and AUDDC (AGPv2 coordinates).

REFERENCES

Acemoglu, D. & **Restrepo, P.** (2022) Demographics and automation. *The Review of Economic Studies*, **89**, 1–44.

Afuakwa, J.J. & **Crookston, R.K.** (1984) Using the kernel milk line to visually monitor grain maturity in maize. *Crop Science*, **24**, 687–691.

Alam, M.R., **Nakasathien, S.**, **Molla, M.S.H.**, **Islam, M.A.**, **Maniruzzaman, M.**, **Ali, M.A.** ***et al.*** (2021) Kernel water relations and kernel filling traits in maize (*Zea mays* L.) are influenced by water-deficit condition in a tropical environment. *Frontiers in Plant Science*, **12**, 717178.

Bissoli, G., **Palomino-Schätzlein, M.**, **Planes, M.D.**, **Renard, J.**, **Krätschmer, T.**, **Silva-Dias, C.** ***et al.*** (2025) Prediction of germination in aged seeds and identification of new seed viability biomarkers using NMR metabolomics. *Physiologia Plantarum*, **177**, e70395.

© 2026 The Author(s).

Borrás, L. & **Westgate, M.E.** (2006) Predicting maize kernel sink capacity early in development. *Field Crops Research*, **95**, 223–233.

Bradbury, P.J., **Zhang, Z.**, **Kroon, D.E.**, **Casstevens, T.M.**, **Ramdoss, Y.** & **Buckler, E.S.** (2007) TASSEL: software for association mapping of complex traits in diverse samples. *Bioinformatics*, **23**, 2633–2635.

Brooking, I.R. (1990) Maize ear moisture during grain-filling, and its relation to physiological maturity and grain-drying. *Field Crops Research*, **23**, 55–68.

Bu, D.C., **Luo, H.T.**, **Huo, P.P.**, **Wang, Z.H.**, **Zhang, S.**, **He, Z.h.** ***et al.*** (2021) KOBAS-i: intelligent prioritization and exploratory visualization of biological functions for gene enrichment analysis. *Nucleic Acids Research*, **49**, W317–W325.

Capelle, V., **Remoué, C.**, **Moreau, L.**, **Reyss, A.**, **Mahé, A.**, **Massonneau, A.** ***et al.*** (2010) QTLs and candidate genes for desiccation and abscisic acid content in maize kernels. *BMC Plant Biology*, **10**, 2.

Chen, J., **Zeng, B.**, **Zhang, M.**, **Xie, S.**, **Wang, G.**, **Hauck, A.** ***et al.*** (2014) Dynamic transcriptome landscape of maize embryo and endosperm development. *Plant Physiology*, **166**, 252–264.

Cheng, C., **An, L.**, **Li, F.**, **Ahmad, W.**, **Aslam, M.**, **Ul Haq, M.Z.** ***et al.*** (2023) Wide-range portrayal of AP2/ERF transcription factor family in maize (*Zea mays* L.) development and stress responses. *Genes*, **14**, 194.

Cross, H.Z. (1991) Leaf expansion rate effects on yield and yield components in early maturing maize. *Crop Science*, **31**, 579–583.

Dai, D.W., **Ma, Z.Y.** & **Song, R.T.** (2021) Maize kernel development. *Molecular Breeding*, **41**, 2.

Dai, L.Y., **Cheng, X.R.**, **Chen, Y.H.**, **Niu, J.S.**, **Cai, X.Y.**, **Liu, Y.T.** ***et al.*** (2019) Effects of husk, cob and pericarp characteristics on kernel moisture content in corn during the grain-filling stage. *International Journal of Agriculture Environment and Bioresearch*, **4**, 79–89.

de Givry, S., **Bouchez, M.**, **Chabrier, P.**, **Milan, D.** & **Schiex, T.** (2005) Carhta gene: multipopulation integrated genetic and radiation hybrid mapping. *Bioinformatics*, **21**, 1703–1704.

Dodig, D., **Zoric, M.**, **Knezevic, D.**, **King, S.** & **Surlan-Momirovic, G.** (2008) Genotype × environment interaction for wheat yield in different drought stress conditions and agronomic traits suitable for selection. *Australian Journal of Agricultural Research*, **59**, 536–545.

Emes, M.J., **Bowsher, C.G.**, **Hedley, C.**, **Burrell, M.M.**, **Scrase-Field, E.S.** & **Tetlow, I.J.** (2003) Starch synthesis and carbon partitioning in developing endosperm. *Journal of Experimental Botany*, **54**, 569–575.

Fan, T.L., **Wang, S.Y.**, **Wang, J.H.** & **Yang, Z.** (2014) Relationship of days after pollination and vigor traits on maize seed maturity in Hexi seed production area in China. *Scientia Agricultura Sinica*, **47**, 2960–2970.

Fang, H.M., **Niu, M.M.**, **Shi, S.**, **Liu, H.** & **Zhou, J.** (2019) Effect of harvesting methods and grain moisture content on maize harvesting quality. *Transactions of the Chinese Society of Agricultural Engineering*, **35**, 11–18.

Feng, X., **Meng, Q.**, **Zeng, J.**, **Yu, Q.**, **Xu, D.**, **Dai, X.** ***et al.*** (2022) Genome-wide identification of sucrose non-fermenting-1-related protein kinase genes in maize and their responses to abiotic stresses. *Frontiers in Plant Science*, **13**, 1087839.

Fukao, T., **Xu, K.**, **Ronald, P.C.** & **Bailey-Serres, J.** (2006) A variable cluster of ethylene response factor-like genes regulates metabolic and developmental acclimation responses to submergence in rice. *Plant Cell*, **18**, 2021–2034.

Ganal, M.W., **Durstewitz, G.**, **Polley, A.**, **Bérard, A.**, **Buckler, E.S.**, **Charcosset, A.** ***et al.*** (2011) A large maize (*Zea mays* L.) SNP genotyping array: development and germplasm genotyping, and genetic mapping to compare with the B73 reference genome. *PLoS One*, **6**, e28334.

Gao, S., **Ming, B.**, **Li, L.L.**, **Hou, L.Y.**, **Wang, K.R.**, **Zhou, S.L.** ***et al.*** (2025) Grain water weight dynamics and their relationships with grain filling in maize. *European Journal of Agronomy*, **164**, 127481.

Gao, S., **Ming, B.**, **Li, L.L.**, **Yin, X.B.**, **Xue, J.**, **Wang, K.R.** ***et al.*** (2021) Relationship and distribution of in-field dry-down and equilibrium in maize grain moisture content. *Agricultural and Forest Meteorology*, **304–305**, 108409.

Gui, S.T., **Wei, W.J.**, **Jiang, C.L.**, **Luo, J.Y.**, **Chen, L.**, **Wu, S.S.** ***et al.*** (2022) A pan-Zea genome map for enhancing maize improvement. *Genome Biology*, **23**, 178.

Han, X., **Zhang, D.**, **Hao, H.**, **Luo, Y.**, **Zhu, Z.** & **Kuai, B.** (2023) Transcriptomic analysis of three differentially senescing maize (*Zea mays* L.) inbred lines upon heat stress. *International Journal of Molecular Sciences*, **24**, 9782.

Hu, Z., **Liu, H.**, **Guo, M.**, **Han, X.**, **Li, Y.**, **Chen, R.** ***et al.*** (2025) Natural variation of an E3 ubiquitin ligase encoding gene Chalk9 regulates grain chalkiness in rice. *Nature Communications*, **16**, 6653.

Jia, T.J., **Wang, L.F.**, **Li, J.J.**, **Ma, J.**, **Cao, Y.Y.**, **Lübberstedt, T.** ***et al.*** (2020) Integrating a genome-wide association study with transcriptomic analysis to detect genes controlling grain drying rate in maize (*Zea mays*, L.). *Theoretical and Applied Genetics*, **133**, 623–634.

Jin, H., **Li, S.** & **Villegas, A.J.** (2006) Down-regulation of the 26S proteasome subunit RPN9 inhibits viral systemic transport and alters plant vascular development. *Plant Physiology*, **142**, 651–661.

Jin, Y., **Wang, Z.H.**, **Chang, H.Z.**, **Wang, L.F.** & **Zhang, Z.C.** (2002) Study on physiological maturity and natural drydown rate in maize. *Journal of Northeast Agricultural University (English Edition)*, **9**, 81–86.

Joehanes, R. & **Nelson, J.C.** (2008) QGene 4.0, an extensible Java QTL-analysis platform. *Bioinformatics*, **24**, 2788–2789.

Keru, W., **Ruizhi, X.**, **Jun, X.**, **Lirong, S.** & **Shaokun, L.** (2022) Comparison and analysis of maize grain commodity quality and mechanical harvest quality between China and the United States. *International Journal of Agricultural and Biological Engineering*, **15**, 55–61.

Kim, D., **Langmead, B.** & **Salzberg, S.L.** (2015) HISAT: a fast spliced aligner with low memory requirements. *Nature Methods*, **12**, 357–360.

Knapp, S.J., **Stroup, W.W.** & **Ross, W.M.** (1985) Exact confidence intervals for heritability on a progeny mean basis. *Crop Science*, **25**, 192–194.

Kosambi, D.D. (2011) The estimation of map distance from recombination values. *Annals of Human Genetics*, **12**, 172–175.

Kovach, D.A. & **Bradford, K.J.** (1992) Imbibitional damage and desiccation tolerance of wild rice (*Zizania palustris*) seeds. *Journal of Experimental Botany*, **43**, 747–757.

Kumar, S., **Stecher, G.**, **Li, M.**, **Knyaz, C.** & **Tamura, K.** (2018) MEGA X: molecular evolutionary genetics analysis across computing platforms. *Molecular Biology and Evolution*, **35**, 1547–1549.

Li, J. & **Ji, L.** (2005) Adjusting multiple testing in multilocus analyses using the eigenvalues of a correlation matrix. *Heredity*, **95**, 221–227.

Li, J.J., **Guo, X.**, **Zhang, M.H.**, **Wang, X.**, **Zhao, Y.**, **Yin, Z.G.** ***et al.*** (2018) OsERF71 confers drought tolerance via modulating ABA signaling and proline biosynthesis. *Plant Science*, **270**, 131–139.

Li, L.L., **Xie, R.Z.**, **Fan, P.P.**, **Lei, X.P.**, **Wang, K.R.**, **Hou, P.** ***et al.*** (2016) Study on dehydration in kernel between Zhengdan958 and Xianyu335. *Journal of Maize Sciences*, **24**, 57–6171.

Li, M.Y., **Peng, G.Y.**, **Deng, B.** & **Meng, G.Y.** (2017) Research progress of rice vascular bundle. *Plant Physiology Journal*, **53**, 1586–1590.

Li, W.Q., **Yu, Y.H.**, **Wang, L.X.**, **Luo, Y.**, **Peng, Y.**, **Xu, Y.C.** ***et al.*** (2021) The genetic architecture of the dynamic changes in grain moisture in maize. *Plant Biotechnology Journal*, **19**, 1195–1205.

Li, X., **Suo, F.**, **Li, Z.**, **Yang, Y.**, **Hao, X.**, **Sun, Q.** ***et al.*** (2025) Kernel dehydration characteristics is related to kernel microstructure and starch granule size distribution in different maize varieties. *Agronomy*, **15**, 2471.

Liao, Y., **Smyth, G.K.** & **Shi, W.** (2014) featureCounts: an efficient general purpose program for assigning sequence reads to genomic features. *Bioinformatics*, **30**, 923–930.

Lin, S.Y., **Lin, Y.L.**, **Usharani, R.**, **Radjacommare, R.** & **Fu, H.** (2024) The structural role of RPN10 in the 26S proteasome and an RPN2-binding residue on RPN13 are functionally important in Arabidopsis. *International Journal of Molecular Sciences*, **25**, 11650.

Liu, D.T., **Wang, Z.**, **Yan, D.W.** & **Xiong, F.** (2017) Advances in the pathway and visualization study of water transport in grain. *Plant Physiology Journal*, **53**, 1947–1954.

Liu, J.J., **Yu, H.**, **Liu, Y.L.**, **Deng, S.N.**, **Liu, Q.C.**, **Liu, B.S.** ***et al.*** (2020) Genetic dissection of grain water content and dehydration rate related to mechanical harvest in maize. *BMC Plant Biology*, **20**, 118.

Liu, Y.C., **Ao, M.**, **Lu, M.**, **Zheng, S.B.**, **Zhu, F.B.**, **Ruan, Y.Y.** ***et al.*** (2023) Genomic selection to improve husk tightness based on genomic molecular markers in maize. *Frontiers in Plant Science*, **14**, 1252298.

Miller, J. & **Gordon, C.** (2005) The regulation of proteasome degradation by multi-ubiquitin chain binding proteins. *FEBS Letters*, **579**, 3224–3230.

Mizik, T., **Nagy, J.**, **Molnár, E.M.** & **Maró, Z.M.** (2025) Challenges of employment in the agrifood sector of developing countries—a systematic literature review. *Humanities & Social Sciences Communications*, **12**, 62.

Müller, M. & **Munné-Bosch, S.** (2015) Ethylene response factors: a key regulatory hub in hormone and stress signaling. *Plant Physiology*, **169**, 32–41.

© 2026 The Author(s).

Null, R.C.T.R., **Team, R.**, **Null, R.C.T.**, **Core Writing, T.**, **Null, R.**, **Team, R.** ***et al.*** (2011) R: a language and environment for statistical computing. *Computing*, **1**, 12–21.

Pan, X.Y. & **Tang, X.Y.** (2018) Research advances on 19S proteasome regulatory subunits in plants. *Plant Physiology Journal*, **54**, 1373–1383.

Park, J.M., **Park, C.J.**, **Lee, S.B.**, **Ham, B.K.**, **Shin, R.** & **Paek, K.H.** (2001) Overexpression of the tobacco Tsi1 gene encoding an EREBP/AP2-type transcription factor enhances resistance against pathogen attack and osmotic stress in tobacco. *Plant Cell*, **13**, 1035–1046.

Purdy, J.L. & **Crane, P.L.** (1967) Inheritance of drying rate in "mature" corn (*Zea mays* L.). *Crop Science*, **7**, 294–297.

Qi, H., **Liang, K.**, **Ke, Y.**, **Wang, J.**, **Yang, P.**, **Yu, F.** ***et al.*** (2023) Advances of Apetala2/ethylene response factors in regulating development and stress response in maize. *International Journal of Molecular Sciences*, **24**, 5416.

Qian, Y.L., **Zhang, X.Q.**, **Wang, L.F.**, **Chen, J.**, **Chen, B.R.**, **Lv, G.H.** ***et al.*** (2016) Detection of QTLs controlling fast kernel dehydration in maize (*Zea mays* L.). *Genetics and Molecular Research*, **15**, gmr15039076.

Qu, J.Z., **Zhong, Y.Y.**, **Ding, L.**, **Liu, X.X.**, **Xu, S.T.**, **Guo, D.W.** ***et al.*** (2022) Biosynthesis, structure and functionality of starch granules in maize inbred lines with different kernel dehydration rate. *Food Chemistry*, **368**, 130796.

Sakuma, Y., **Liu, Q.**, **Dubouzet, J.G.**, **Abe, H.**, **Shinozaki, K.** & **Yamaguchi-Shinozaki, K.** (2002) DNA-binding specificity of the ERF/AP2 domain of Arabidopsis DREBs, transcription factors involved in dehydration- and cold-inducible gene expression. *Biochemical and Biophysical Research Communications*, **290**, 998–1009.

Sala, R.G., **Andrade, F.H.** & **Cerono, J.C.** (2012) Quantitative trait loci associated with grain moisture at harvest for line per se and testcross performance in maize: a meta-analysis. *Euphytica*, **185**, 429–440.

Shibahara, T., **Kawasaki, H.** & **Hirano, H.** (2002) Identification of the 19S regulatory particle subunits from the rice 26S proteasome. *European Journal of Biochemistry*, **269**, 1474–1483.

Trinh Thi, V.H. & **Zhou, W.Q.** (2024) A systematic analysis of the development of agricultural modernization and its effect on crop production in northeastern China. *Sustainability*, **16**, 5055.

US Grains Council. (2026) Corn harvest quality report 2025/2026. https://grains.org/corn_report/corn-harvest-quality-report-2025-2026/

Wang, F., **Shen, K.** & **Cai, Y.** (2025) When the abundance ends: economic transformation, population aging, and shrinking lifecycle surplus in China. *The Journal of the Economics of Ageing*, **30**, 100544.

Wang, K.R., **Li, L.L.**, **Gao, S.**, **Wang, Y.Z.**, **Huang, Z.F.**, **Xie, R.Z.** ***et al.*** (2021) Analysis of main quality index of corn harvesting with combine in China. *Acta Agronomica Sinica*, **47**, 2440–2449.

Wang, W., **Ren, Z.B.**, **Li, L.**, **Du, Y.P.**, **Zhou, Y.Y.**, **Zhang, M.C.** ***et al.*** (2022) Meta-QTL analysis explores the key genes, especially hormone related genes, involved in the regulation of grain water content and grain dehydration rate in maize. *BMC Plant Biology*, **22**, 346.

Wang, X., **Gomes, M.M.**, **Bailly, C.**, **Nambara, E.** & **Corbineau, F.** (2021) Role of ethylene and proteolytic N-degron pathway in the regulation of Arabidopsis seed dormancy. *Journal of Integrative Plant Biology*, **63**, 2110–2122.

Wang, Y., **Long, T.**, **Qin, A.**, **Liao, Q.**, **Wang, H.**, **Zhang, J.** ***et al.*** (2025) ABA-activated subclass III SnRK2s control kernel maturation in maize. *The Crop Journal*, **13**, 777–791.

Widdicombe, W.D. & **Thelen, K.D.** (2002) Row width and plant density effects on corn grain production in the northern corn belt. *Agronomy Journal*, **94**, 1020–1023.

Xie, R.-z., **Ming, B.**, **Gao, S.**, **Wang, K.-r.**, **Hou, P.** & **Li, S.-k.** (2022) Current state and suggestions for mechanical harvesting of corn in China. *Journal of Integrative Agriculture*, **21**, 892–897.

Xin, S.L., **Zhao, W.Y.**, **Qu, H.**, **Yang, T.**, **Shi, R.J.**, **Yan, Z.B.** ***et al.*** (2024) Current situation analysis and development trend of maize mechanized harvesting technology. *Journal of Agricultural Mechanization Research*, **46**, 9–14.

Xu, Z.S., **Chen, M.**, **Li, L.C.** & **Ma, Y.Z.** (2011) Functions and application of the AP2/ERF transcription factor family in crop improvement. *Journal of Integrative Plant Biology*, **53**, 570–585.

Yang, H.J., **Shen, H.**, **Chen, L.**, **Xing, Y.Y.**, **Wang, Z.Y.**, **Zhang, J.L.** ***et al.*** (2002) The OsEBP-89 gene of rice encodes a putative EREBP transcription factor and is temporally expressed in developing endosperm and intercalary meristem. *Plant Molecular Biology*, **50**, 379–391.

Yang, J., **Carena, M.J.** & **Uphaus, J.** (2010) Area under the dry down curve (AUDDC): a method to evaluate rate of dry down in maize. *Crop Science*, **50**, 2347–2354.

Yang, N., **Lu, Y.**, **Yang, X.H.**, **Huang, J.**, **Zhou, Y.**, **Ali, F.** ***et al.*** (2014) Genome wide association studies using a new nonparametric model reveal the genetic architecture of 17 agronomic traits in an enlarged maize association panel. *PLoS Genetics*, **10**, e1004573.

Yang, Z.Y., **Lyu, S.Q.**, **Li, J.**, **Li, H.T.**, **Wang, X.F.** & **Wang, L.Q.** (2023) Effects of nitrogen, variety and planting density on the mechanized harvest characters and yield of spring maize. *Transactions of the Chinese Society of Agricultural Engineering*, **39**, 41–50.

Yang, Z.Z., **Li, Y.L.** & **Wu, C.T.** (2025) Population aging, fintech, and agricultural economic resilience. *International Review of Economics and Finance*, **97**, 103756.

Yin, S.Y., **Liu, J.**, **Yang, T.T.**, **Li, P.C.**, **Xu, Y.**, **Fang, H.M.** ***et al.*** (2020) Genetic analysis of the seed dehydration process in maize based on a logistic model. *Crop Journal*, **8**, 182–193.

Yu, Y.H., **Li, W.Q.**, **Liu, Y.F.**, **Liu, Y.J.**, **Zhang, Q.Z.**, **Ouyang, Y.D.** ***et al.*** (2025) A *Zea* genus-specific micropeptide controls kernel dehydration in maize. *Cell*, **188**, 44–59.e21.

Zeng, Z.B. (1994) Precision mapping of quantitative trait loci. *Genetics*, **136**, 1457–1468.

Zhang, J., **Zhang, F.Q.**, **Tang, B.J.**, **Ding, Y.**, **Xia, L.K.**, **Qi, J.S.** ***et al.*** (2020) Molecular mapping of quantitative trait loci for grain moisture at harvest and field grain drying rate in maize (*Zea mays* L.). *Physiologia Plantarum*, **169**, 64–72.

Zhang, Y., **Li, J.**, **Chen, S.**, **Ma, X.**, **Wei, H.**, **Chen, C.** ***et al.*** (2020) An APETALA2/ethylene responsive factor, OsEBP89 knockout enhances adaptation to direct-seeding on wet land and tolerance to drought stress in rice. *Molecular Genetics and Genomics*, **295**, 941–956.

Zhang, Z., **Ersoz, E.**, **Lai, C.Q.**, **Todhunter, R.J.**, **Tiwari, H.K.**, **Gore, M.A.** ***et al.*** (2010) Mixed linear model approach adapted for genome-wide association studies. *Nature Genetics*, **42**, 355–360.

Zhou, G.F., **Mao, Y.X.**, **Xue, L.**, **Chen, G.Q.**, **Lu, H.H.**, **Shi, M.L.** ***et al.*** (2020) Genetic dissection of husk number and length across multiple environments and fine-mapping of a major-effect QTL for husk number in maize (*Zea mays* L.). *The Crop Journal*, **8**, 1071–1080.

© 2026 The Author(s).